Angewandte Chemie
Eine Zeitschrift der Gesellschaft Deutscher Chemiker

Supporting Information

69451 Weinheim, Germany

CO Oxidation Catalyzed by Supported Gold: Cooperation between Gold and Nanocrystalline Rare Earth Supports Forms Reactive Surface Superoxide and Peroxide Species**

Javier Guzman, Silvio Carrettin, Juan C. Fierro-Gonzalez, Yalin Hao, Bruce C. Gates, and Avelino Corma*

1. Catalysts characterization prior to reaction.

1a. X-ray diffraction (XRD). X-ray powder diffraction data were recorded using a Philips X'Pert diffractometer equipped with a secondary graphite monochromator, operating at 40 kV and 45 mA, provided with a variable divergence slit and working in the fixed irradiated area mode. It was employed a nickel-filtered Cu-K_a radiation (? = 0.1542 nm) and a Bragg–Brentano geometry.

1b. Transmission electron microscopy (TEM). Transmission electron microscopy images were obtained on a Jeol 1200X electron microscope operating at 120 keV. The samples for TEM analysis were prepared directly by dispersion of the powder sample onto carbon copper grids.

1c. N_2 adsorption–desorption. The nitrogen adsorption and desorption isotherms were measured at 77 K using an ASAP 2010 system from Micromeritics. The samples were pretreated under vacuum at 673 K overnight. The surface

area of the samples was determined from the BET (Brunner–Emmett–Teller) model.

1d. CO–temperature-programmed reduction–mass spectrometry (CO–TPR–MS). Temperature-programmed reduction experiments were performed with a Micromeritics AutoChem 2910 catalyst characterization system; it was equipped with a thermal conductivity detector (TCD). Mass spectra of the off-gases were measured online with a Balzers ThermoStar™ mass spectrometer running in multi-ion monitoring mode. Prior to each experiment, the sample was pretreated at room temperature in flowing He [10 mL (NTP) min^{-1}] for 20 min. The sample powder was treated by heating from 298 to 923 K at a rate of 5 K min^{-1} in a flow of 5 vol % CO in He. The total gas flow rate was 50 mL (NTP) min^{-1}.

1e. X-ray photoelectron spectra (XPS). XPS data were collected in a VG Escalab 210 spectrometer using monochromated Al Ka (*h?* = 1486.6 eV) X-ray radiation. To avoid photoreduction of ceria, the energy of the X-ray beam was limited to 100 W. Kinetic energies of photoelectrons were measured with a hemispherical electron analyzer working at constant pass energy of 50 eV. The pressure in the analyzing chamber was maintained at 750 × 10^{-6} Torr. The binding energy scales were corrected by setting the C1s transition at 284.5 eV.

2. Operando characterization during CO oxidation catalysis.

2a. Infrared (IR) spectroscopy. A BioRad spectrometer with a spectral resolution of 2 cm^{-1} was used to collect transmission infrared spectra of the solid catalysts. Samples were pressed (~ 2 ton/cm^2 for 5 minutes) into self-supporting wafers and loaded into the cell connected to a vaccum/adsorption system, which allowed recording of the spectra while the treatment gas was adsorbed/desorbed from the samples during experiments. The catalysts were pretreated at 323 K in vacuum (10^{-2} Pa) for 1 h before adsorption experiments. Adsorption of CO, O_2, or CO + O_2 was performed at room temperature. Each reported spectrum is the average of 64 scans.

2b. Raman spectroscopy. Raman spectra were collected with a Renishaw inVia Raman spectrometer equipped with a Leica DMLM microscope and a 514-nm Ar^+ ion laser as an excitation source. A × 50 objective of 8-mm optical length was used to focus the depolarized laser beam on a spot of about 2 μm in diameter, and using a laser power at the sample of 2.0 mW. The Raman scattering was collected with a CCD array detector and in the 100–1700 cm^{-1} spectral region with a resolution of 2 cm^{-1}. Each reported spectrum is the average of 20 scans with an exposure time each of 10 s. O_2 and CO adsorption and CO oxidation experiments were

conducted in an in situ cell (Linkam Scientific, THMS 600). Samples were pressed (~ 2 ton/cm^2 for 5 minutes) into self-supporting wafers and loaded into the cell connected to a vaccum/adsorption system, which allowed recording of the spectra while the treatment gas was adsorbed/desorbed from the samples during experiments. The catalysts were pretreated at 323 K in vacuum (10^{-2} Pa) for 1 h before adsorption experiments.

2c. X-ray absorption spectroscopy (XAS). The X-ray absorption spectroscopy experiments were performed at beamline X-18B at the National Synchrotron Light Source (NSLS), Brookhaven National Laboratory, Upton, NY. The storage ring electron energy was 2.5 GeV, and the ring current varied within the range of 110–250 mA. Spectra were collected in the fluorescence mode, which was chosen rather than the transmission mode because of the high absorbance by Ce at the Au L_{III} edge (11919 eV). Higher harmonics in the X-ray beam were minimized by detuning the Si(111) double crystal monochromator by 20–25% at the Au L_{III} edge (11919 eV). The Ge detector with 13 channels allowed recording of 13 signals per scan, and each reported spectrum is the average of seven scans. Data were recorded during CO oxidation catalysis at 298 K and also with the catalysts in flowing He at atmospheric pressure and at a temperature in the range of 298–373 K. In an Ar-filled

drybox at the synchrotron, 0.3 g of powder sample was loaded into a XAS cell/reactor (the powder catalyst was held in the middle of a XAS cell/reactor by glass wool plugs), which was then isolated, removed from the glove box, and installed in the flow system at the beamline without contacting of the catalyst with air or moisture. The XAS cell/reactor is well approximated as a plug-flow reactor.

Analysis of the EXAFS data was carried out with a difference file technique by use of the software XDAP. No attempt was made to account for the small atomic X-ray absorption fine structure (AXAFS) (the low-r portion; r is the distance from the absorber atom, Au) of the spectrum other than by application of standard background subtraction techniques. Iterative fitting was carried out until excellent agreement was attained between the calculated k^0-, k^1-, and k^2-weighted data (k is the photoelectron wave vector) and the postulated model. Experimentally determined reference files prepared from EXAFS data representing materials of known structure were used in the analysis. EXAFS data characterizing a gold foil and $Na_2Pt(OH)_6$ were used for the phase shifts and backscattering amplitudes of the Au–Au and Au–$O_{support}$ interactions. (The transferability of the phase shifts and backscattering amplitudes for neighboring atoms in the

periodic table has been justified experimentally). $Au(CH_3)_2(acac)$ mixed with SiO_2 was used to obtain the phase shifts and backscattering amplitudes for analysis of the Au–C and Au–O interactions. The Au–Ce reference file was calculated by using the code FEFF 7.0 and FEFF 8.0. The number of parameters used in fitting the data to each model is justified statistically by the Nyquist theorem. The fitting ranges in both momentum space and real space were determined by the data quality. The quality of the fitting was confirmed by the values of fit diagnostic parameters, $e_?^2$ (goodness of fit) and the variances between the data and model predictions for the EXAFS function χ and the Fourier transform of χ (for k^0-, k^1- and , k^2- weighting of the data). The X-ray absorption edge energy was calibrated with the measured signal of a gold foil (at the Au L_{III} edge, 11919 eV) scanned simultaneously with the sample. The edge is represented as the inflection point at the first absorption peak, at nearly 11919 eV. The data were normalized by dividing the absorption intensity by the height of the absorption edge.

3. Supplementary results.

We find that the characteristics of the cerium oxide surface are extremely important in determining whether a CeO_2-supported gold catalyst is active or not for CO oxidation. When the reaction was carried out at 283 K, the activity of our gold (2.8 weight per cent) on nanostructured CeO_2 catalyst was 2.2×10^{-6} mol_{CO} s^{-1} g_{cat}^{-1}. However, when we placed gold (2.8 weight per cent) on a regular CeO_2 support prepared by precipitation (S_{BET} = 70 m^2 g^{-1}), the specific rate was almost two orders of magnitude lower (CO conversion 1.8 %)[12]. Therefore, the fact that the CeO_2 support is in the form of nanostructured particles appears to be a key factor for achieving high activity in the oxidation of CO to CO_2 when Au is placed on a support. IR spectroscopy characterizing CO adsorption on gold supported on nanostructured CeO_2 demonstrate the presence of Au^{3+}, Au^{+}, and Au^{0} species as indicated by their characteristic Au^{x}–CO frequency at 2148, 2130, and 2104 cm^{-1}, respectively (see below). Interestingly, during CO adsorption experiments and without any oxygen in the gas stream, CO_2 was formed. This result indicates that nanostructured CeO_2 is able to supply reactive oxygen to the gold active species for the oxidation of CO, consistent with the idea of CeO_2 acting as an oxygen buffer by releasing–uptaking oxygen through redox processes involving the Ce^{4+}/Ce^{3+} couple. In contrast, when gold was deposited

on regular CeO_2, only Au^0 and a small fraction of Au^+ species were detected. Furthermore, no CO_2 formation was detected during CO adsorption experiments. XPS and XANES results confirm our assignments of gold oxidation states in the Au/CeO_2 samples, and provide evidence of the presence of Ce^{+3} ions on the surface of the nanocrystalline CeO_2–supported gold catalyst (see below).

Supporting Information Table 1: XPS results characterizing gold supported on regular and nanocrystalline CeO_2 supports

Sample	B.E. Au $4f_{7/2}$ [eV]	Assignment	B.E. Ce $3d_{5/2}$ [eV]	Assignment
Au/CeO_2-nanocrystalline	86.2	Au^{3+}		
	84.7	Au^{+}		
			880.4	Ce^{3+}
			884.0	Ce^{4+}
Au/CeO_2-regular	84.1	Au^{0}		
			884.0	Ce^{4+}
Au foil	84.0	Au^{0}		

Supporting Information Table 2: EXAFS parameters characterizing gold supported on nanocrystalline CeO_2 catalysts and the species formed from them during CO oxidation catalysis at 298 K.[†]

Gold loading in the catalyst (wt%)	shell	Scanning Conditions: He at 298 K				Scanning Conditions: CO oxidation catalysis[‡]			
		N	*R* (Å)	$?s^2 \times 10^3$ (Å^2)	$?E_0$ (eV)	*N*	*R* (Å)	$?s^2 \times 10^3$ (Å^2)	$?E_0$ (eV)
0.92	1st Au–Au	0.8	2.77	6.04	–2.28	2.7	2.79	7.89	–1.60
	2nd Au–Au	–	–	–	–	0.8	4.04	1.88	0.43
	Au–Ce	0.6	3.25	0.91	–6.26	0.9	3.23	1.97	3.25
	$Au–O_s$	3.7	2.04	0.02	0.92	0.1	2.48	–13.0	2.27
	$Au–O_l$	2.3	3.69	0.27	–1.59	0.9	3.69	0.45	–0.63
1.28	1st Au–Au	–	–	–	–	–	–	–	–
	2nd Au–Au	–	–	–	–				
	Au–Ce	0.8	3.01	11.2	1.94				
	$Au–O_s$	3.5	2.00	0.01	9.39				
	$Au–O_l$	3.0	3.66	1.89	0.69				
1.73	1st Au–Au	–	–	–	–	3.0	2.79	14.80	–1.48
	2nd Au–Au	–	–	–	–	–	–	–	–
	Au–Ce	1.2	3.09	12.98	–6.15	0.1	3.22	–5.37	–0.52
	$Au–O_s$	3.0	2.00	0.01	7.1(	2.9	2.04	0.27	2.47
	$Au–O_l$	3.7	3.64	0.02	1.1[	2.9	3.66	3.11	0.44
2.80	1st Au–Au	4.1	2.84	6.28	–3.17	4.1	2.83	4.82	–1.14

	2nd Au–Au	1.7	4.06	8.69	0.61	2.5	4.04	8.77	3.98
	Au–Ce	0.1	3.02	–1.10	–1.02	0.3	2.99	–0.34	1.43
	$Au–O_s$	1.0	2.02	–2.01		1.5	2.06	10.73	–2.23
					7.31				
	$Au–O_l$	1.3	3.66	2.03	–0.41	1.0	3.51	–0.39	12.83
4.65	1st Au–Au	4.8	2.82	6.86	–0.75	5.9	2.82	8.06	–1.27
	2nd Au–Au	3.0	4.08	7.82	–1.25	3.0	4.11	7.10	–6.29
	Au–Ce	0.1	3.21	2.00	9.42	0.1	3.20	1.41	1.00
	$Au–O_s$	0.8	2.05	0.27	2.60	0.2	2.11	–3.12	–0.76
	$Au–O_l$	–	–	–	–	–	–	–	–

† N = coordination number; R = distance between absorber and backscatterer atoms; $?s^2$ = Debye–Waller factor; $?E_0$ = inner potential correction. The subscripts s = short and l = long. Typical errors are as follows: N ± 10%, R ± 0.02 Å, $?s^2$ ± 20%, $?E_0$ ± 20%. ‡ Catalytic reaction conditions stated in the Experimental Section.

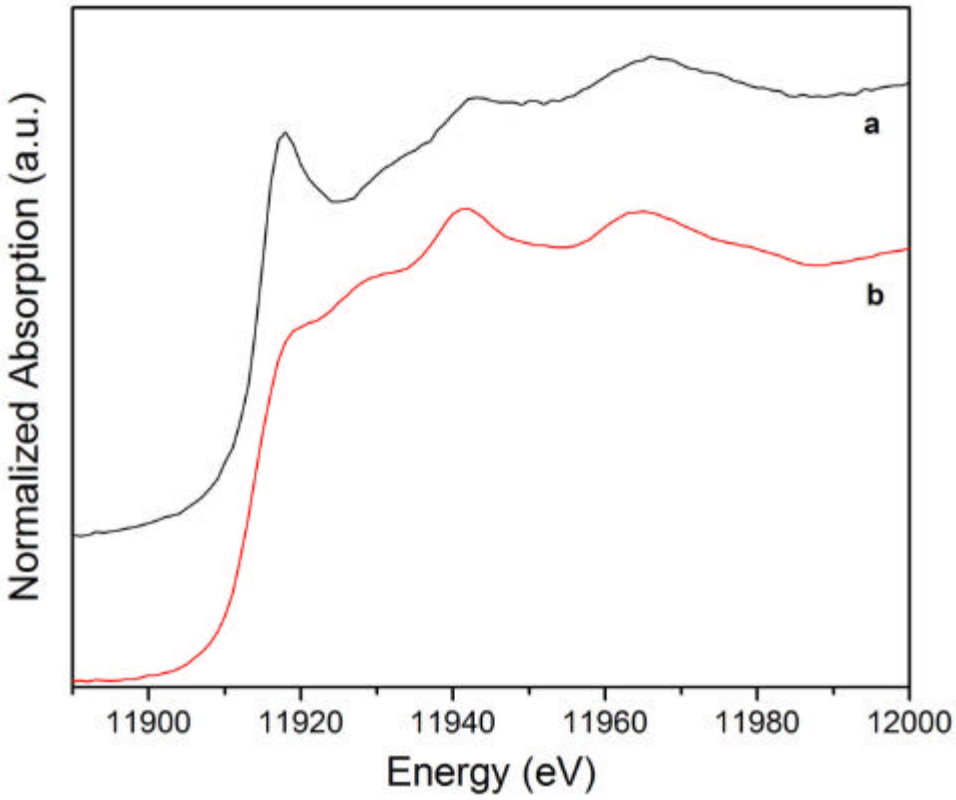

Supporting Information Figure 1. XANES data characterizing 2.8 weight per cent gold supported on (a) nanocrystalline CeO_2 and (b) regular CeO_2.

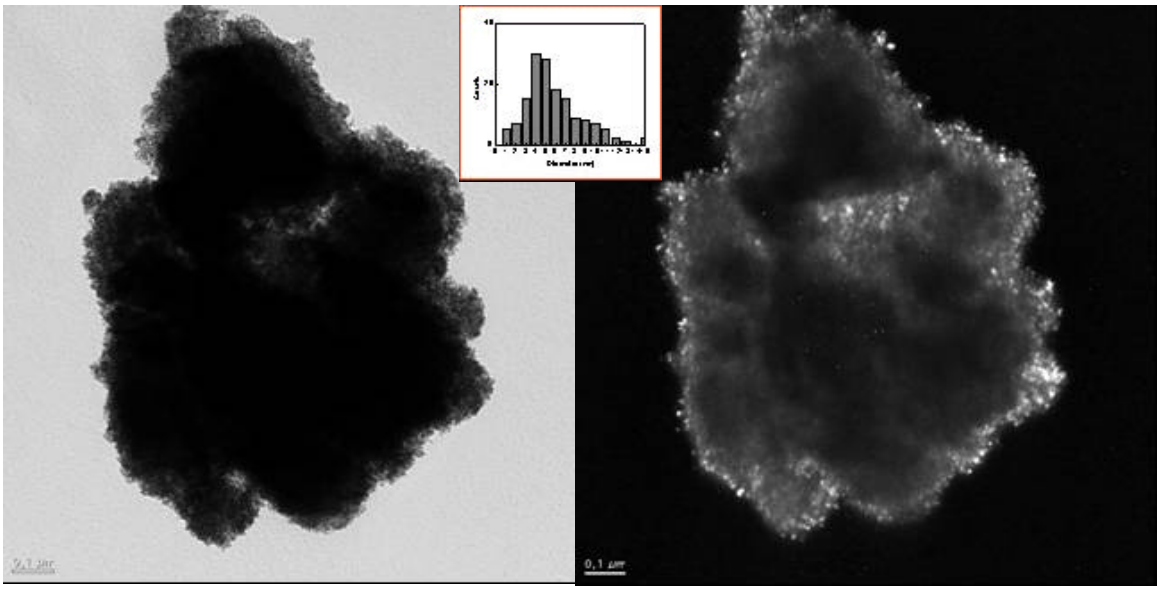

Supporting Information Figure 2. Bright filed (left) and dark field (right) TEM images characterizing 2.8 weight per cent gold supported on nanocrystalline CeO_2. The brighter spots on the right picture correspond to Au crystals with the 111 direction perpendicular to the sample plane. The inset figure shows the size distribution histogram of the gold nanoparticles on the nanocrystalline CeO_2 matrix. The gold average particle size is 4 nm.

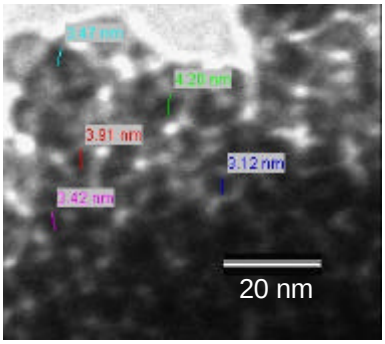

Supporting Information Figure 3. Bright filed TEM image characterizing 2.8 weight per cent gold supported on regular CeO_2. The gold average particle size is 4 nm.

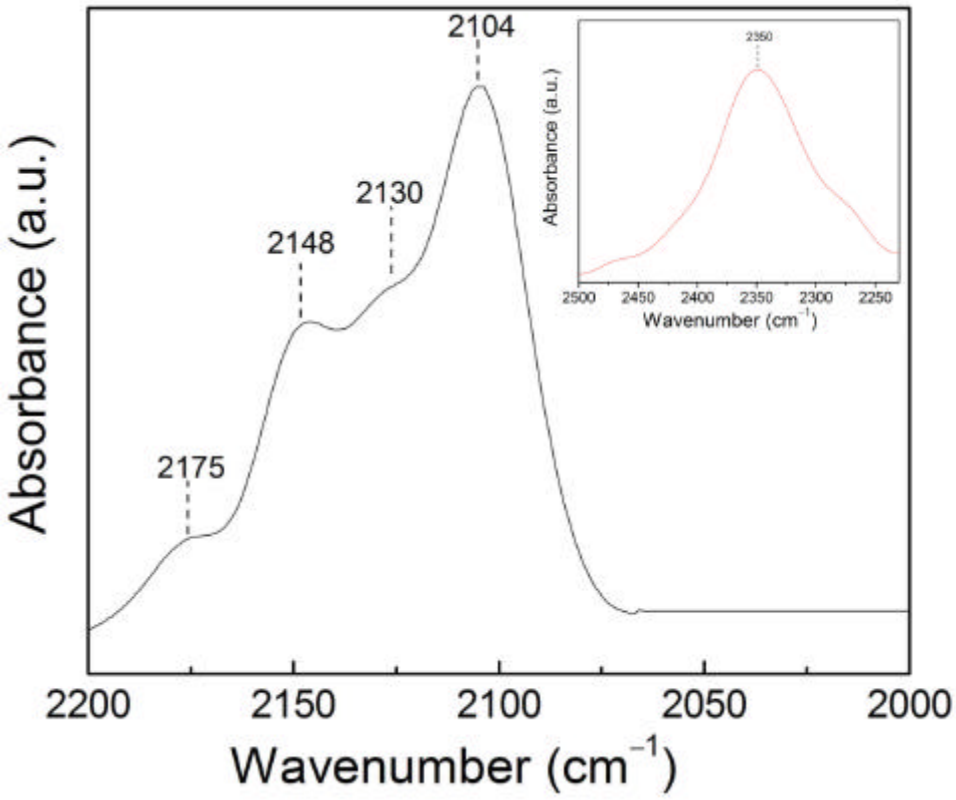

Supporting Information Figure 4. FTIR spectra of CO adsorbed on gold supported on nanocrystalline CeO_2 at a CO pressure of 30 Torr and at room temperature. The inset shows the band representing CO_2 formation.

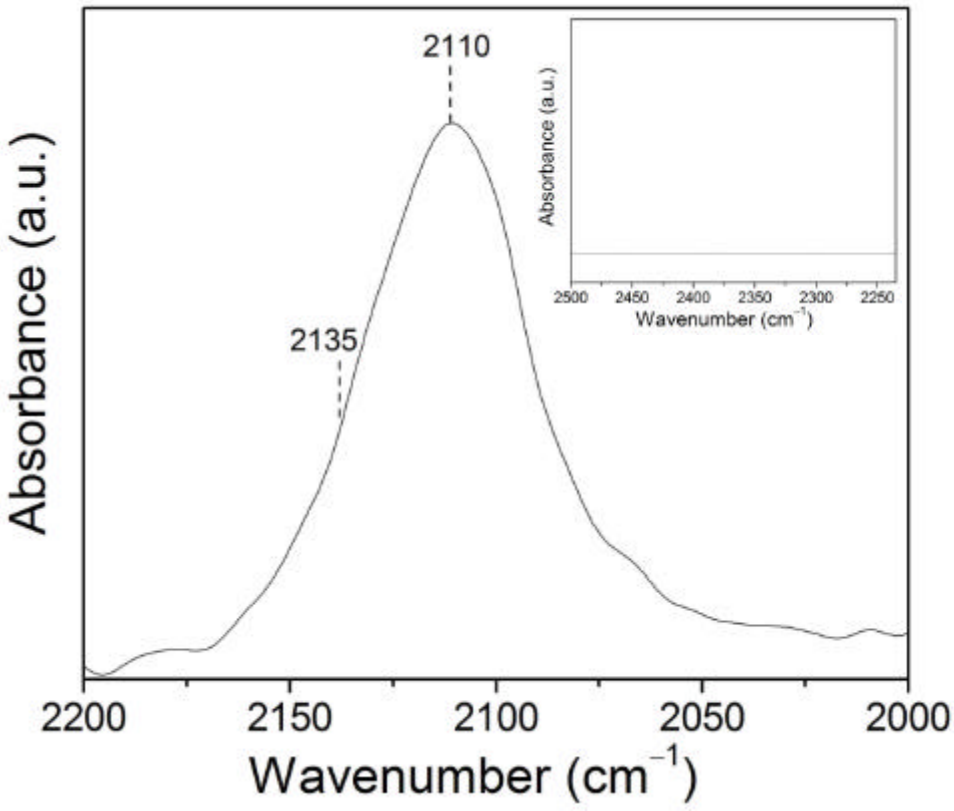

Supporting Information Figure 5. FTIR spectra of CO adsorbed on gold supported on regular CeO_2 at a CO pressure of 30 Torr and at room temperature. The inset shows the region of the expected CO_2 formation.

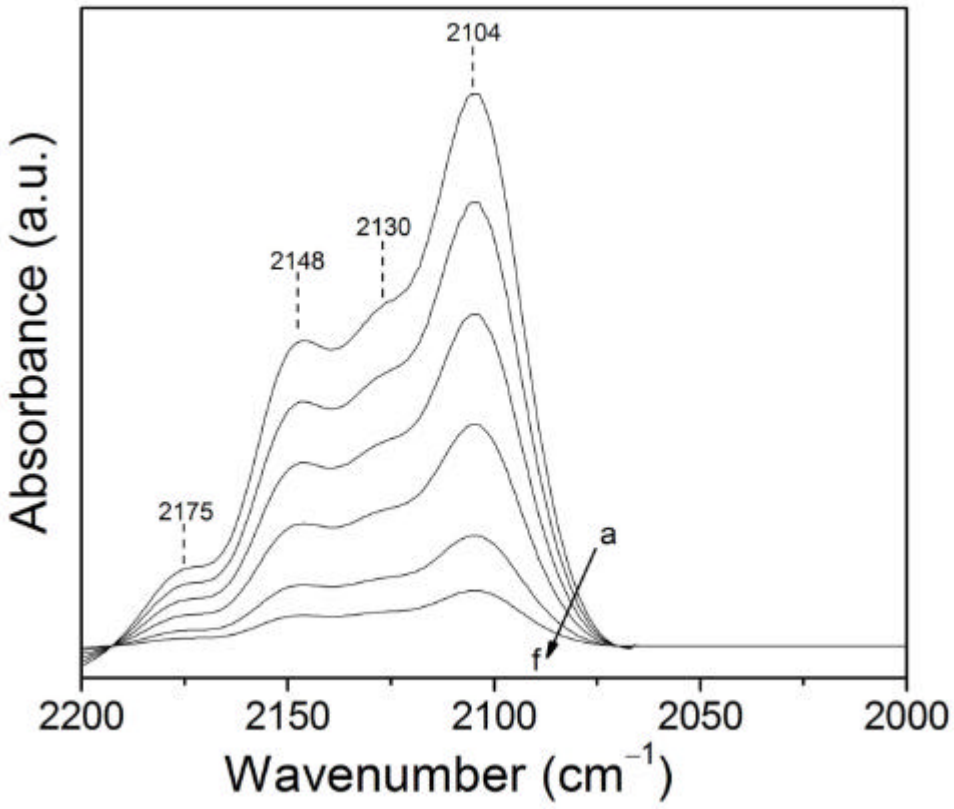

Supporting Information Figure 6. FTIR spectra of 40 Torr of CO adsorbed on gold supported on nanocrystalline CeO_2 at room temperature and subsequent reaction with O_2; time-resolved spectra after O_2 admission ($CO:O_2$ molar ratio of 3) at a) 1 min; b) 5 min; c) 10 min; d) 15 min; e) 20 min; and f) 30 min.

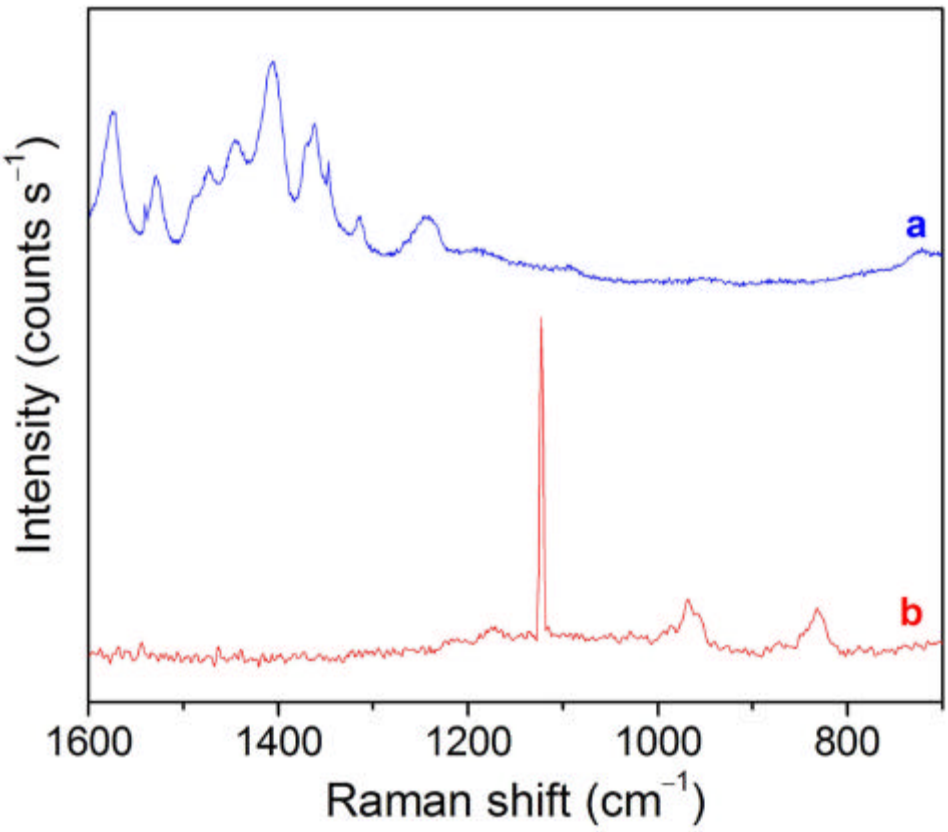

Supporting Information Figure 7. Raman spectra characterizing O_2 adsorbed on (a) regular CeO_2 and (b) nanocrystalline CeO_2.

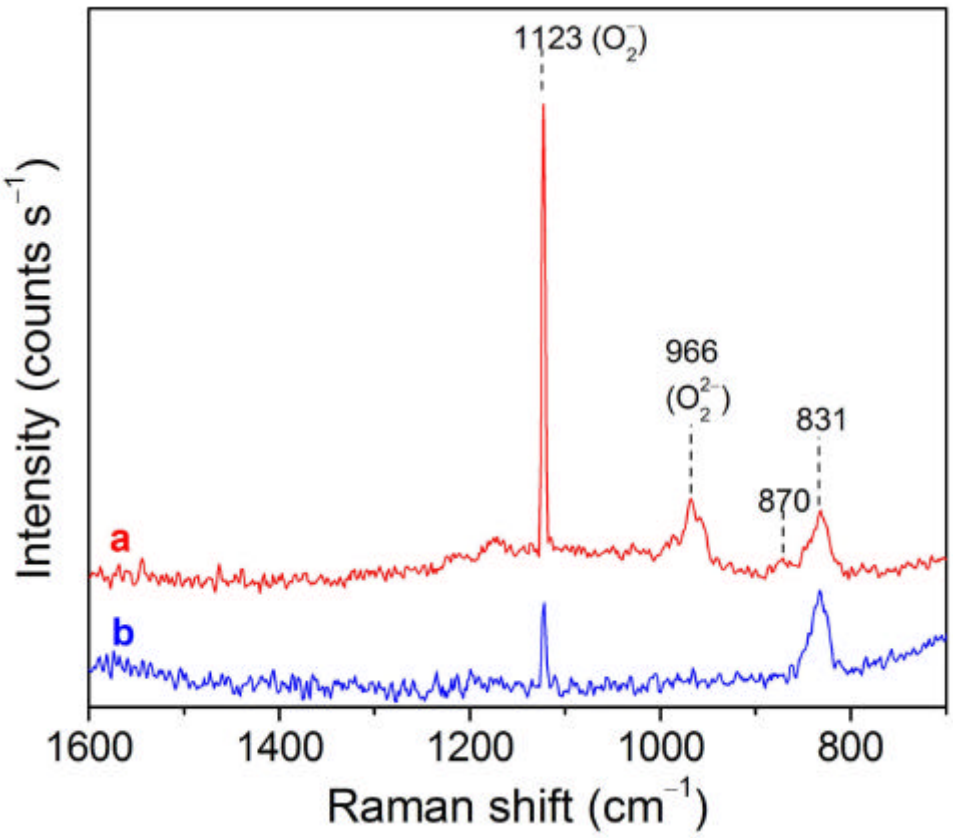

Supporting Information Figure 8. Raman spectra characterizing the 2.8 weight per cent gold supported on nanocrystalline CeO_2 (a) before and (b) during steady-state CO oxidation reaction.

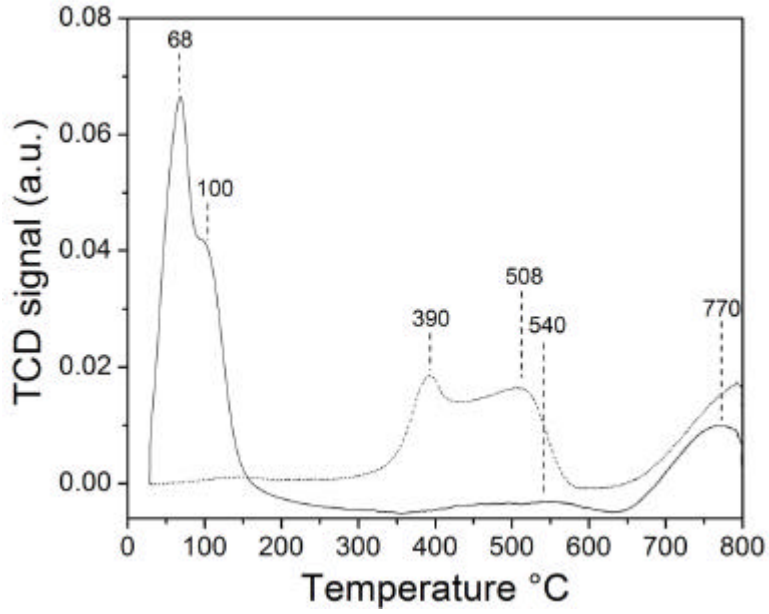

Supporting Information Figure 9. H_2–TPR profile characterizing the gold supported on nanocrystalline CeO_2 (solid line) and nanocrystalline CeO_2 samples (dashed line). Experimental conditions: 0.01 g of catalyst; 5 mole % H_2 in He; 50 ml min^{-1}; and ramping the temperature from 20 to 800 °C at a rate of 3 °C min^{-1}.

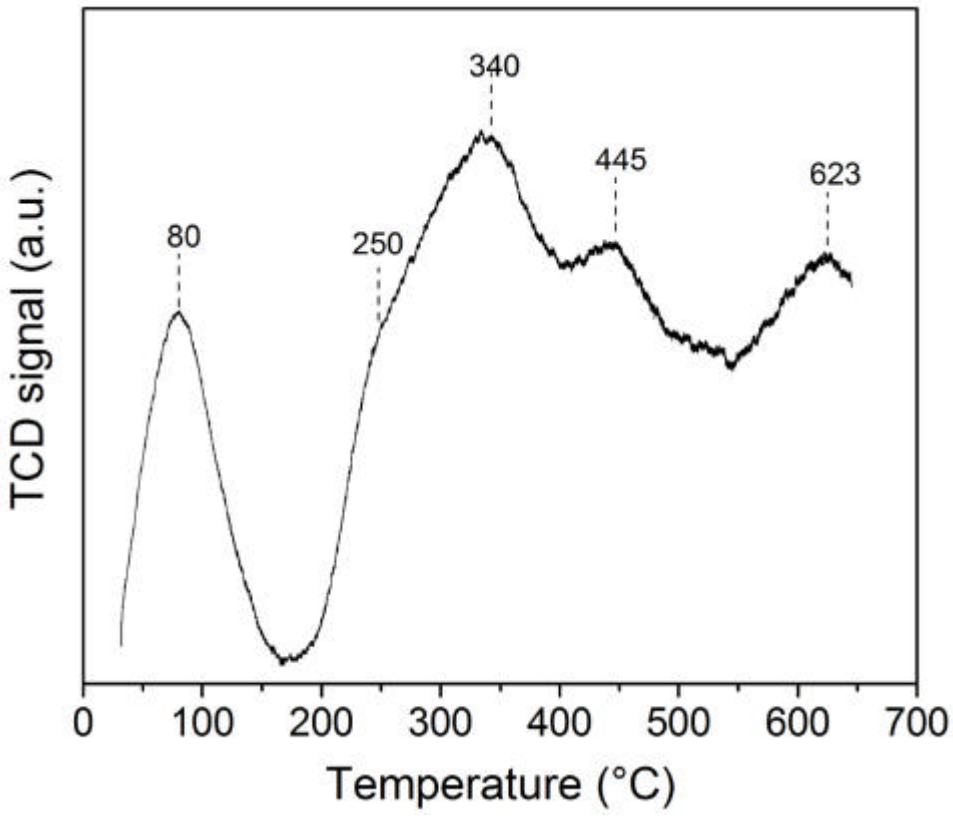

Supporting Information Figure 10. CO–TPR profile characterizing the gold supported on nanocrystalline CeO_2 sample. Experimental conditions: 0.01 g of catalyst; 5 mole % CO in He; 100 ml min^{-1}; and ramping the temperature from 20 to 650 °C at a rate of 3 °C min^{-1}.

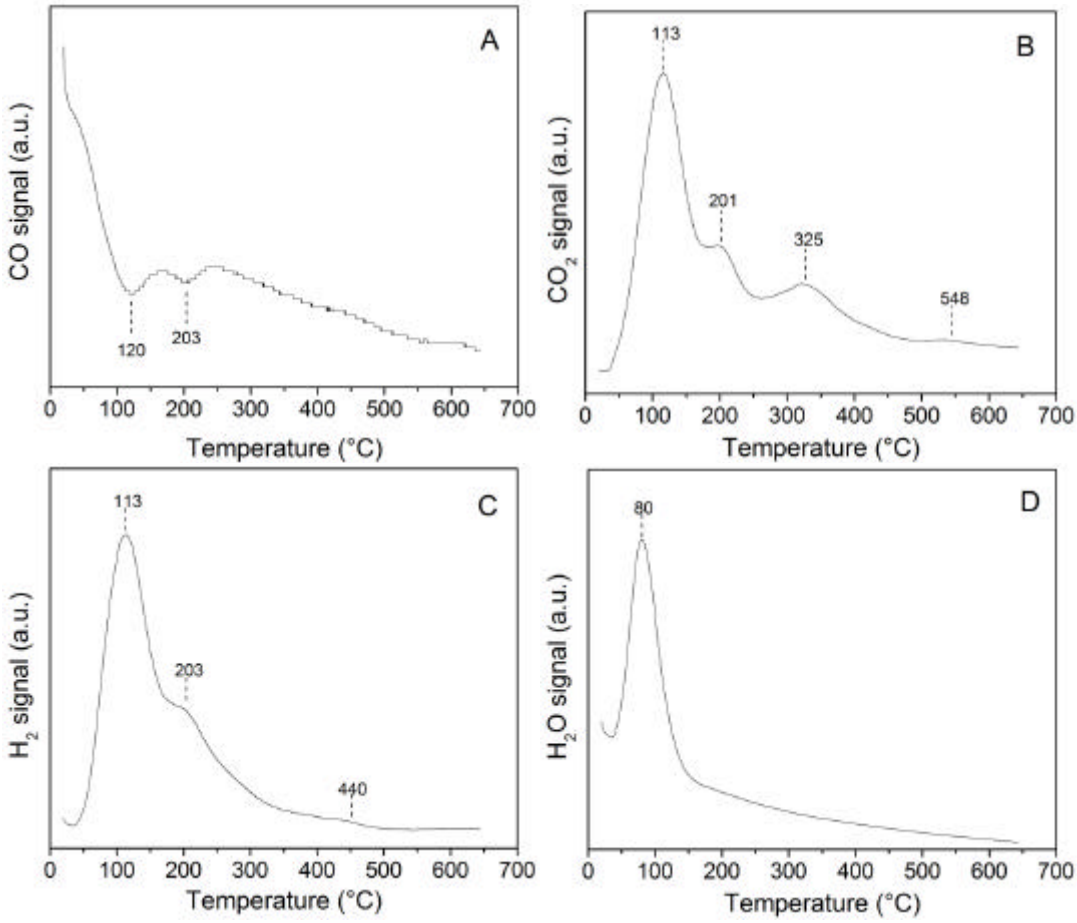

Supporting Information Figure 11. Mass spectrometry of evolved gases during CO–TPR characterization of the 2.8 weight per cent gold supported on nanocrystalline CeO_2 sample; measuring: (A) CO consumption; (B) CO_2 formation; (C) H_2 formation; and (D) H_2O formation.

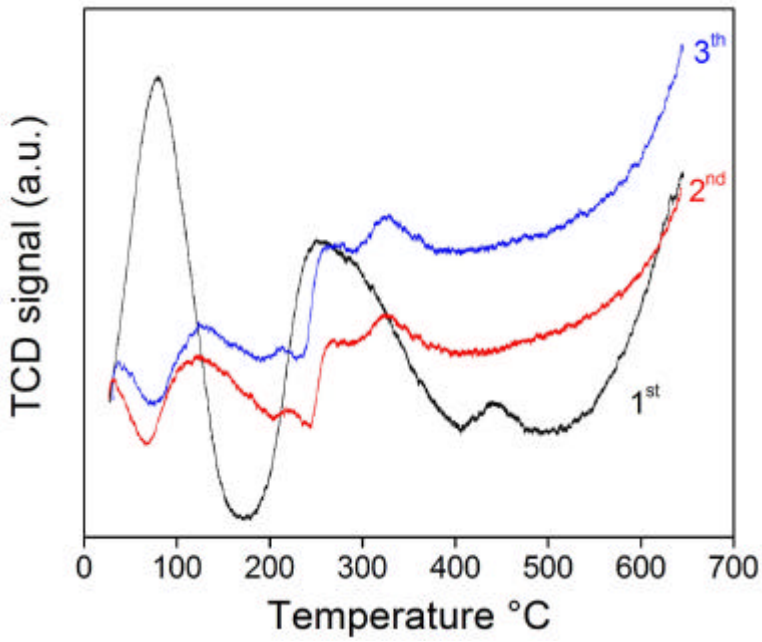

Supporting Information Figure 12. Cyclic CO-TPR experiments of the gold supported on nanocrystalline CeO_2 sample. Experimental conditions: 0.01 g of catalyst; 5 mole % CO in He; 100 ml min^{-1}; and ramping the temperature from 20 to 650 °C at a rate of 3 °C min^{-1}; after each TPR, the sample was oxidized in a stream of 20% O_2 in He at 300 °C for 1 hr, then purged in He at room temperature for 1 hr.

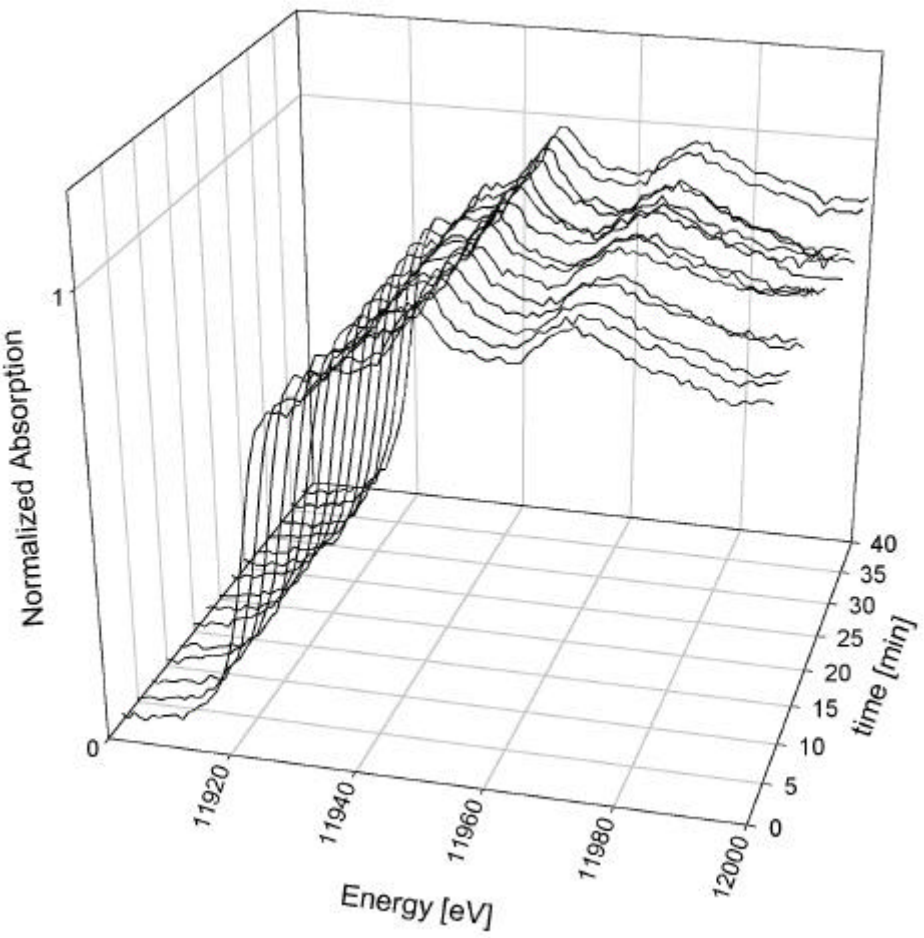

Supporting Information Figure 13. Time-resolved operando XANES data characterizing 2.8 weight per cent gold supported on regular CeO_2 during CO oxidation catalysis at 298 K and 1 atm.

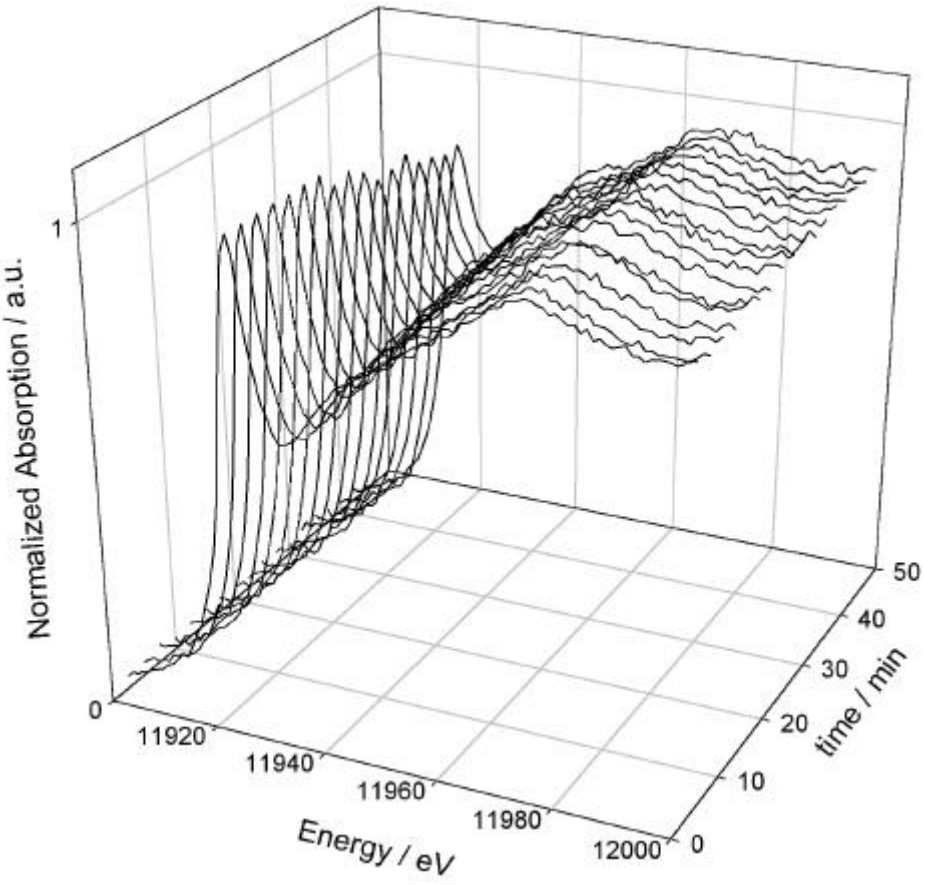

Supporting Information Figure 14. Time-resolved operando XANES data characterizing 0.92 weight per cent gold supported on nanocrystalline CeO_2 during CO oxidation catalysis at 298 K and 1 atm.

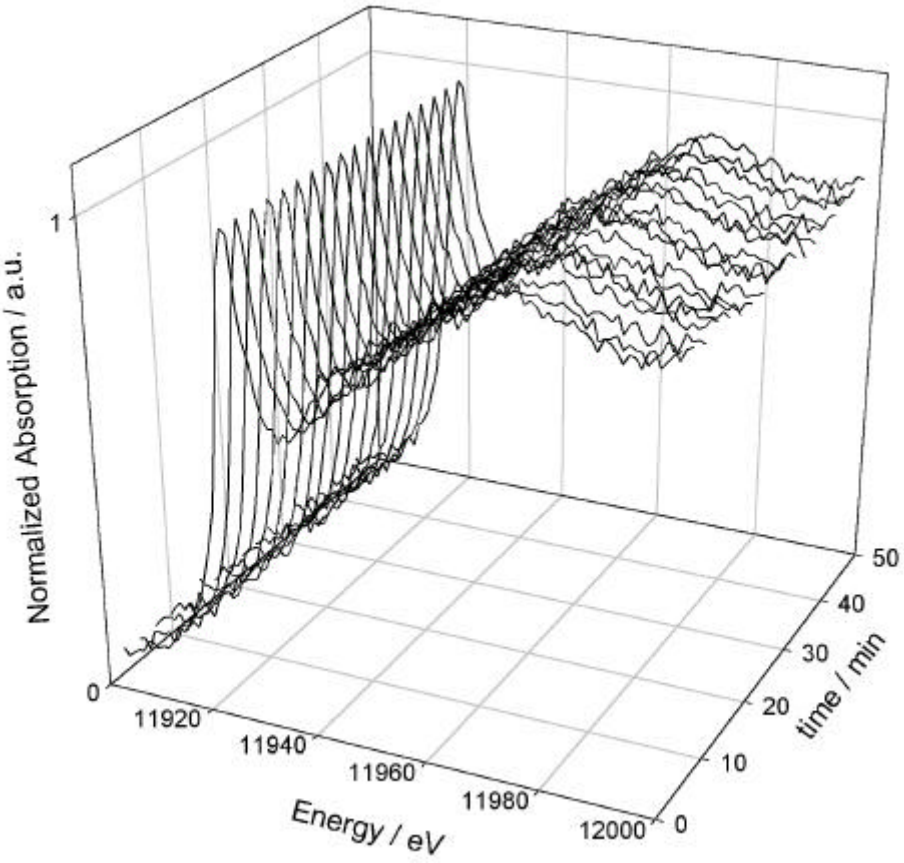

Supporting Information Figure 15. Time-resolved operando XANES data characterizing 1.28 weight per cent gold supported on nanocrystalline CeO_2 during CO oxidation catalysis at 298 K and 1 atm.

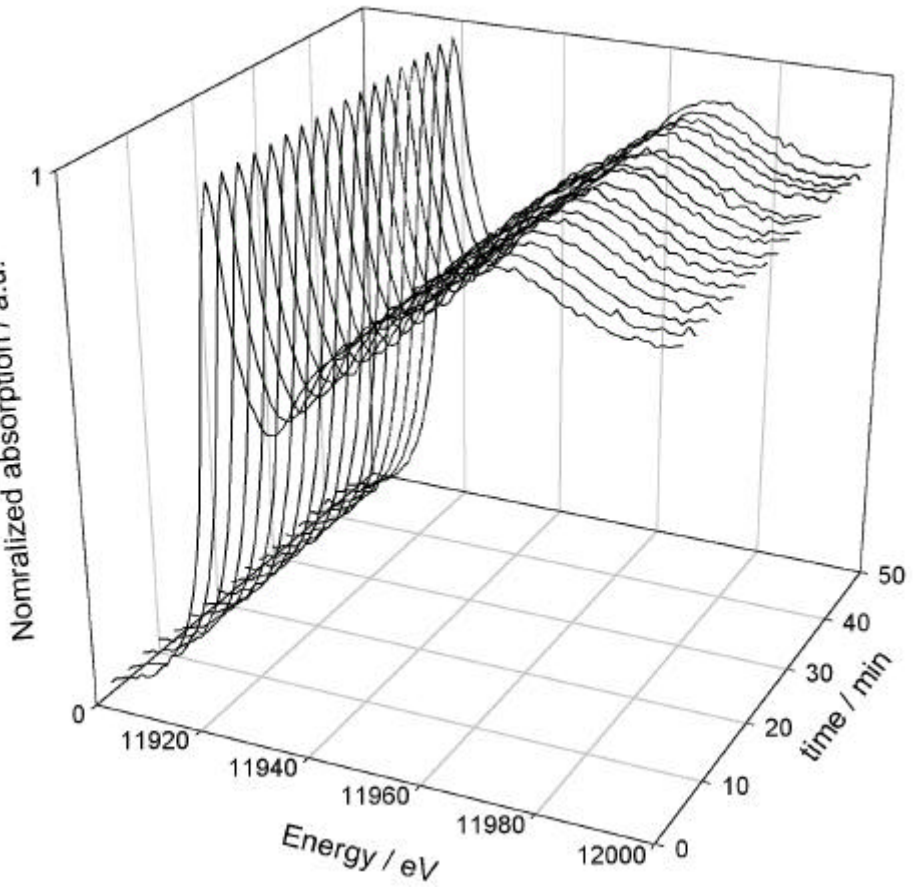

Supporting Information Figure 16. Time-resolved operando XANES data characterizing 1.73 weight per cent gold supported on nanocrystalline CeO_2 during CO oxidation catalysis at 298 K and 1 atm.

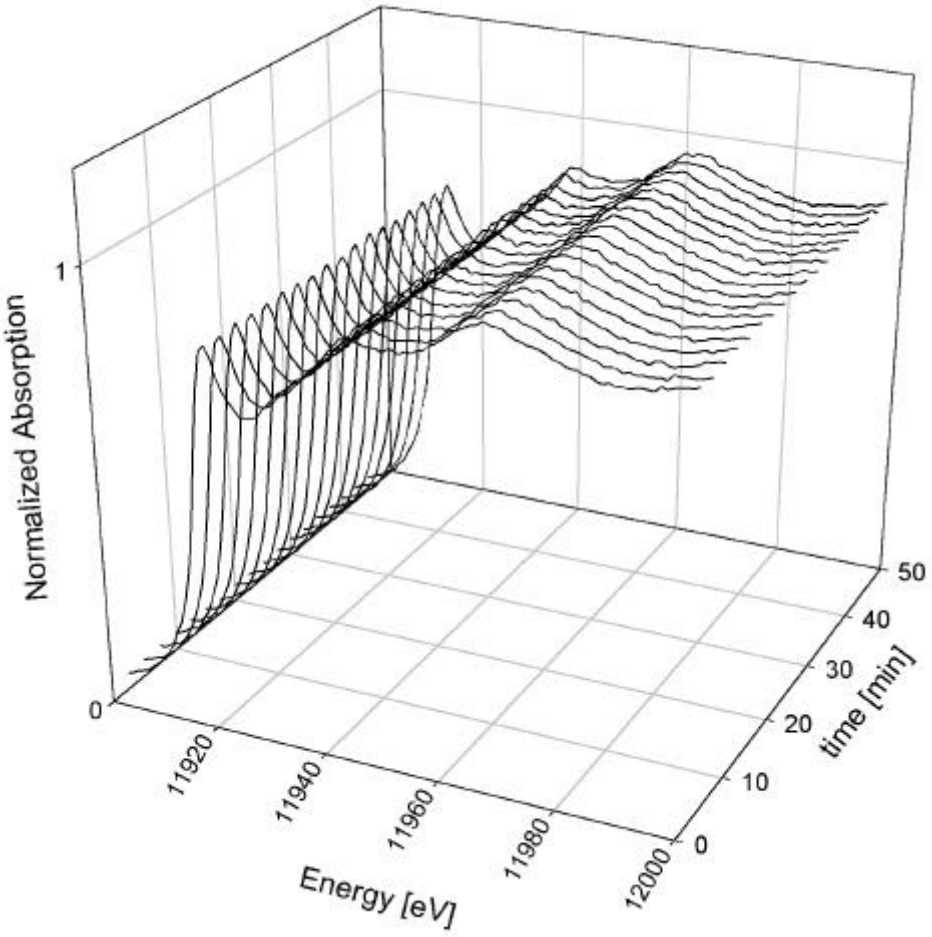

Supporting Information Figure 17. Time-resolved operando XANES data characterizing 2.8 weight per cent gold supported on nanocrystalline CeO_2 during CO oxidation catalysis at 298 K and 1 atm.

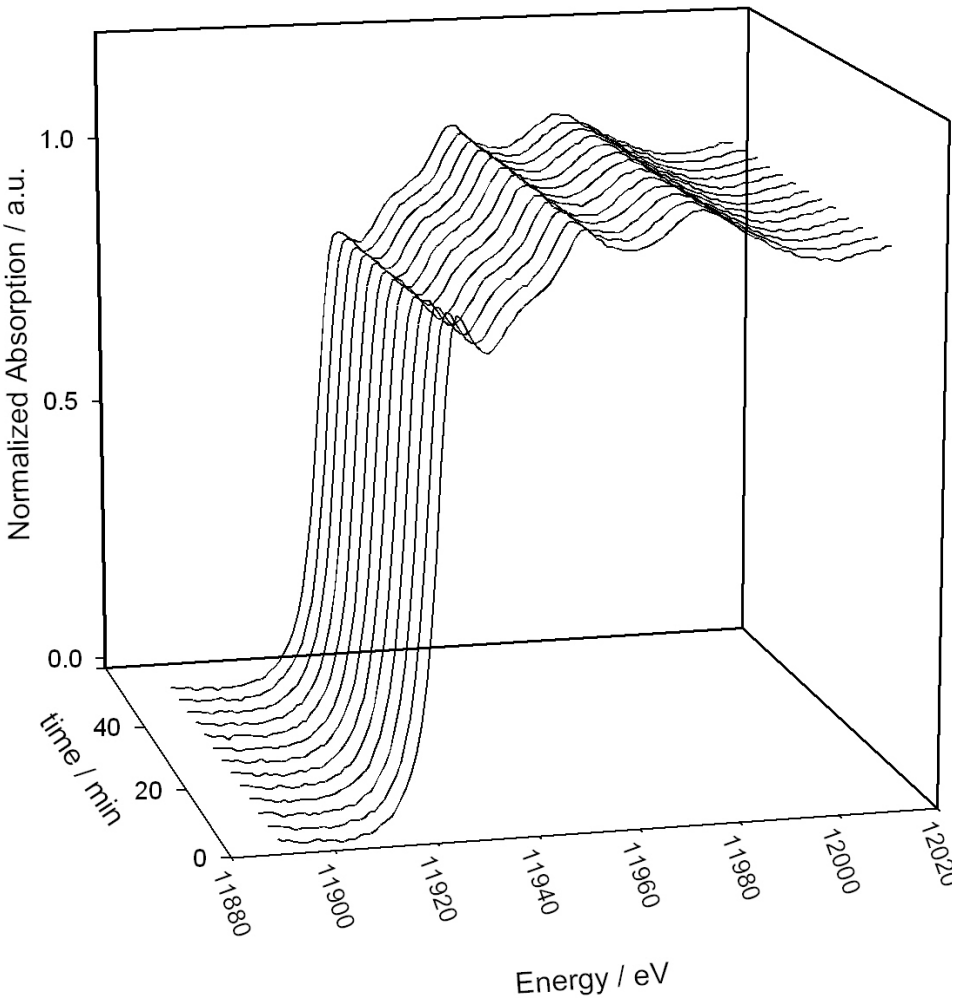

Supporting Information Figure 18. Time-resolved operando XANES data characterizing 4.65 weight per cent gold supported on nanocrystalline CeO_2 during CO oxidation catalysis at 298 K and 1 atm.

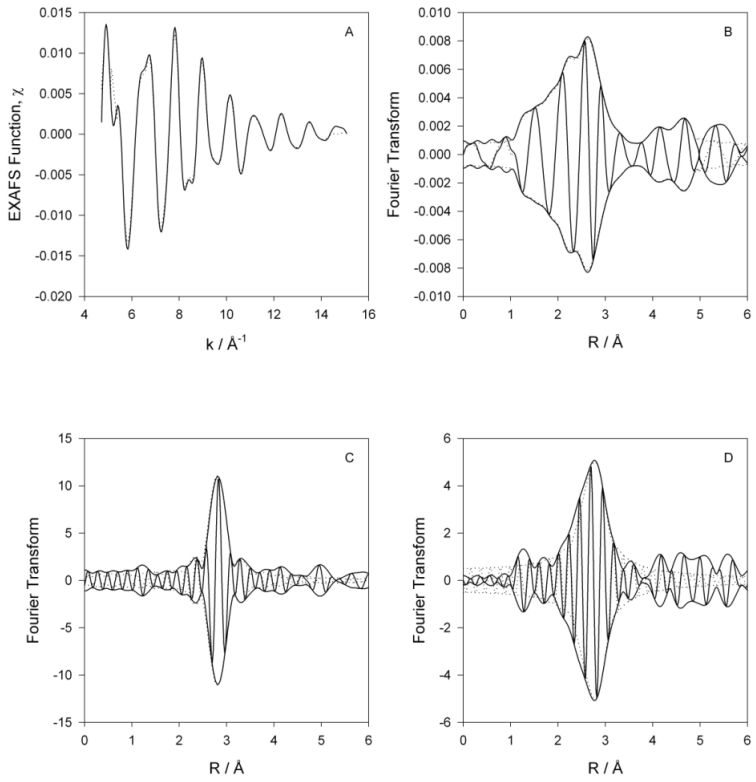

Supporting Information Figure 19. Results of EXAFS analysis characterizing 2.8 weight per cent gold supported on regular CeO_2 during He treatment at 298 K and 1 atm. (A) Experimental EXAFS function (solid line) and sum of the calculated Au–Au + Au–O_l + Au–Ce contributions (dashed line). (B) Imaginary part and magnitude of uncorrected Fourier Transform (k^0 weighted) of experimental EXAFS function (solid line) and sum of the calculated Au–Au + Au–O_l + Au–Ce contributions (dashed line). (C) Residual spectrum illustrating the Au–Au contribution; imaginary part and magnitude of phase- and amplitude-corrected Fourier transform (k^0 weighted) of experimental data minus the calculated Au–O_l + Au–Ce contributions (solid line) and calculated Au–Au contribution (dashed line). (D) Residual spectrum illustrating the Au–O_l contribution; imaginary

part and magnitude of phase- and amplitude-corrected Fourier transform (k^0 weighted) of experimental data minus the calculated Au–Au + Au–Ce contributions (solid line) and calculated $Au–O_l$ contribution (dashed line).

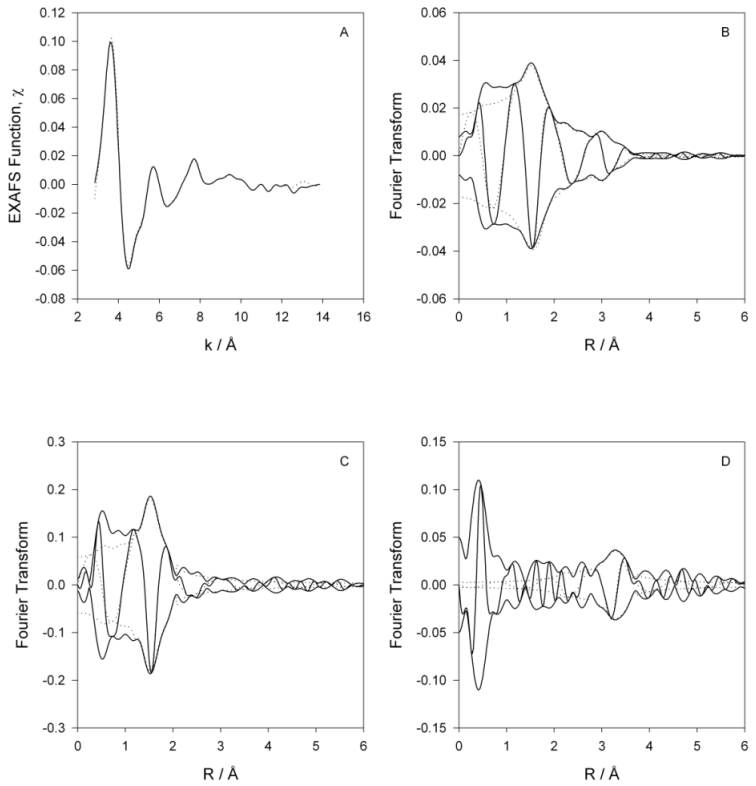

Supporting Information Figure 20. Results of EXAFS analysis characterizing 0.92 weight per cent gold supported on nanocrystalline CeO_2 during He treatment at 298 K and 1 atm. (A) Experimental EXAFS function (solid line) and sum of the calculated Au–Au + Au–O_s + Au–O_l + Au–Ce contributions (dashed line). (B) Imaginary part and magnitude of uncorrected Fourier Transform (k^0 weighted) of experimental EXAFS function (solid line) and sum of the calculated Au–Au + Au–O_s + Au–O_l + Au–Ce contributions (dashed line). (C) Residual spectrum illustrating the Au–O_s contribution; imaginary part and magnitude of phase- and amplitude-corrected Fourier transform (k^0 weighted) of experimental data minus the calculated Au–Au + Au–O_l + Au–Ce contributions (solid line) and calculated Au–O_s contribution (dashed line). (D) Residual spectrum

illustrating the Au–O_l contribution; imaginary part and magnitude of phase- and amplitude-corrected Fourier transform (k^0 weighted) of experimental data minus the calculated Au–Au + Au–O_s + Au–Ce contributions (solid line) and calculated Au–O_l contribution (dashed line).

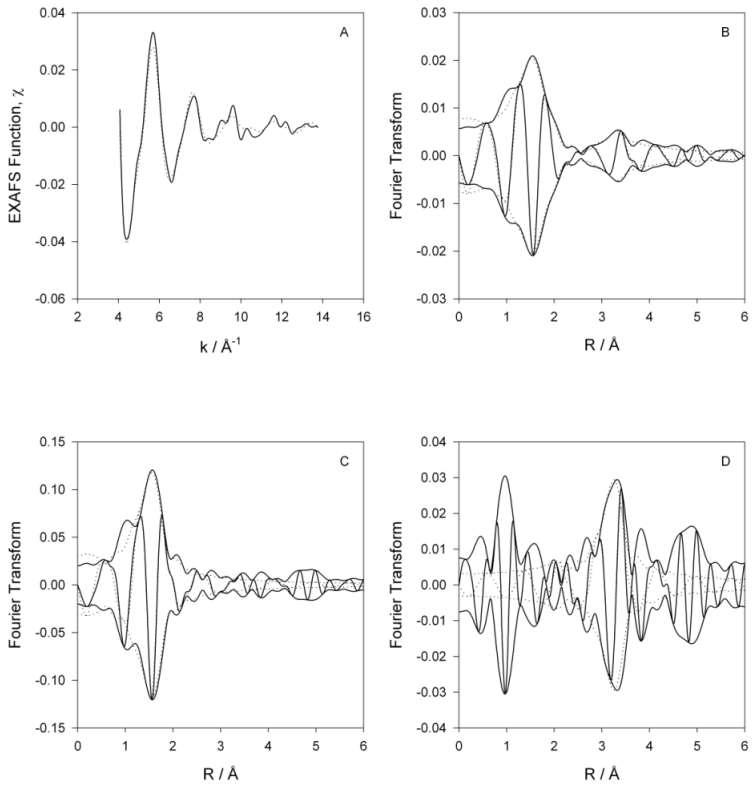

Supporting Information Figure 21. Results of EXAFS analysis characterizing 1.28 weight per cent gold supported on nanocrystalline CeO_2 during He treatment at 298 K and 1 atm. (A) Experimental EXAFS function (solid line) and sum of the calculated Au–Au + Au–O_s + Au–O_l + Au–Ce contributions (dashed line). (B) Imaginary part and magnitude of uncorrected Fourier Transform (k^0 weighted) of experimental EXAFS function (solid line) and sum of the calculated Au–Au + Au–O_s + Au–O_l + Au–Ce contributions (dashed line). (C) Residual spectrum illustrating the Au–O_s contribution; imaginary part and magnitude of phase- and amplitude-corrected Fourier transform (k^0 weighted) of experimental data minus the calculated Au–Au + Au–O_l + Au–Ce contributions (solid line) and calculated Au–O_s contribution (dashed line). (D) Residual spectrum

illustrating the Au–O_l contribution; imaginary part and magnitude of phase- and amplitude-corrected Fourier transform (k^0 weighted) of experimental data minus the calculated Au–Au + Au–O_s + Au–Ce contributions (solid line) and calculated Au–O_l contribution (dashed line).

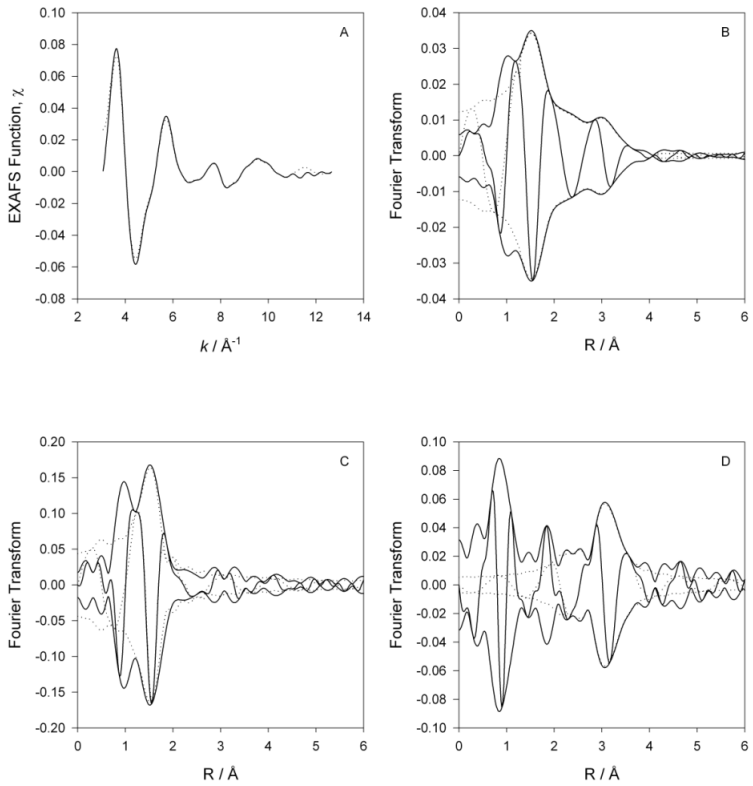

Supporting Information Figure 22. Results of EXAFS analysis characterizing 1.73 weight per cent gold supported on nanocrystalline CeO_2 during He treatment at 298 K and 1 atm. (A) Experimental EXAFS function (solid line) and sum of the calculated Au–Au + Au–O_s + Au–O_l + Au–Ce contributions (dashed line). (B) Imaginary part and magnitude of uncorrected Fourier Transform (k^0 weighted) of experimental EXAFS function (solid line) and sum of the calculated Au–Au + Au–O_s + Au–O_l + Au–Ce contributions (dashed line). (C) Residual spectrum illustrating the Au–O_s contribution; imaginary part and magnitude of phase- and amplitude-corrected Fourier transform (k^0 weighted) of experimental data minus the calculated Au–Au + Au–O_l + Au–Ce contributions (solid line) and calculated Au–O_s contribution (dashed line). (D) Residual spectrum

illustrating the Au–O_l contribution; imaginary part and magnitude of phase- and amplitude-corrected Fourier transform (k^0 weighted) of experimental data minus the calculated Au–Au + Au–O_s + Au–Ce contributions (solid line) and calculated Au–O_l contribution (dashed line).

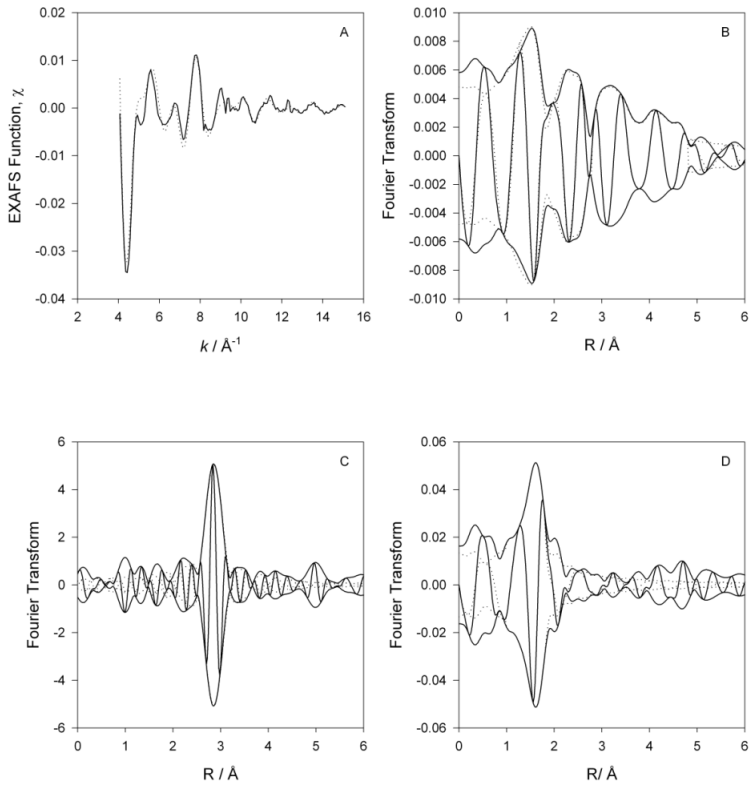

Supporting Information Figure 22. Results of EXAFS analysis characterizing 2.8 weight per cent gold supported on nanocrystalline CeO_2 during He treatment at 298 K and 1 atm. (A) Experimental EXAFS function (solid line) and sum of the calculated Au–Au + Au–O_s + Au–O_l + Au–Ce contributions (dashed line). (B) Imaginary part and magnitude of uncorrected Fourier Transform (k^0 weighted) of experimental EXAFS function (solid line) and sum of the calculated Au–Au + Au–O_s + Au–O_l + Au–Ce contributions (dashed line). (C) Residual spectrum illustrating the Au–Au contribution; imaginary part and magnitude of phase- and amplitude-corrected Fourier transform (k^0 weighted) of experimental data minus the calculated Au–O_s + Au–O_l + Au–Ce contributions (solid line) and calculated Au–Au contribution (dashed line). (D) Residual spectrum

illustrating the Au–O_s contribution; imaginary part and magnitude of phase- and amplitude-corrected Fourier transform (k^0 weighted) of experimental data minus the calculated Au–Au + Au–O_l + Au–Ce contributions (solid line) and calculated Au–O_s contribution (dashed line).

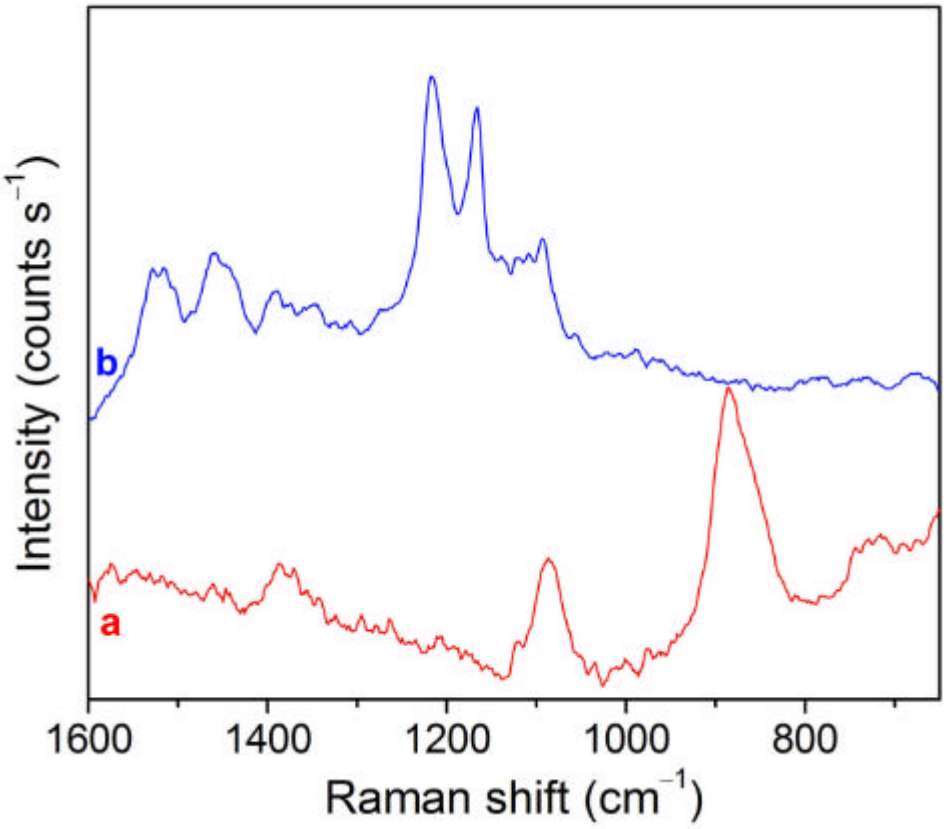

Supporting Information Figure 23. Raman spectra characterizing O_2 adsorbed on (a) nanostructured Y_2O_3 and (b) regular Y_2O_3.

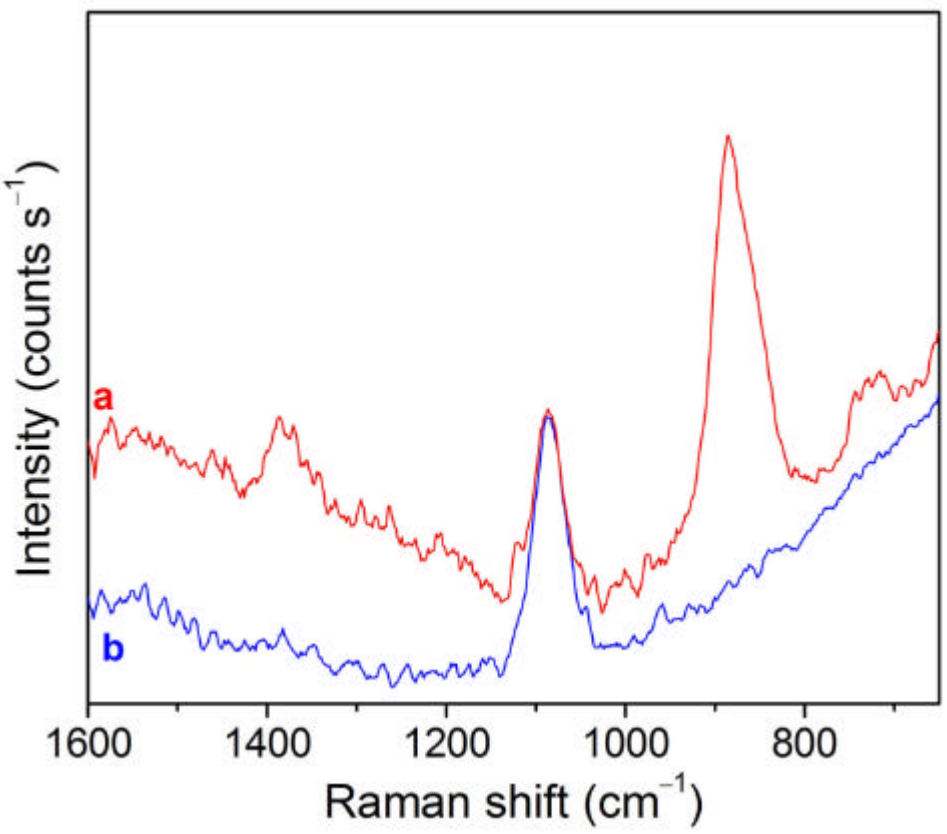

Supporting Information Figure 24. Raman spectra characterizing the 2.5 weight per cent gold supported on nanostructured Y_2O_3 (a) before and (b) during steady-state CO oxidation reaction.